Full Paper

Wiley Online Library

ELECTROANALYSIS

DOI: 10.1002/elan.202060348

New Amine/Phenylglycedyl Ether Adducts for Mild Steel Protection in 1 M HCl: Experimental and Computational Study

C. O. Akalezi,*[a, b] F. C. Onwumere,[a] C. O. Alisa,[a] M. N. Nnanyereugo,[a] and E. E. Oguzie[a, b]

Abstract: The key objective of this study is to ascertain the effect of structure and increased molecular size on the corrosion inhibition potential of two synthesized amines, when compared to their precursor compounds. The product amines were N-(2-hydroxy-3-phenoxy) ethanolamine (NHPE), N,N–Di-(2-hydroxy-3-phenoxypropyl) ethanolamine (NNHPE) synthesized from monoethanolamine (MEA) and phenyl glycidyl ether (PGE) as starting materials. Both starting and product amines were characterized using FTIR spectroscopy. The corrosion inhibition potentials were assessed using experimental and quantum theoretical modeling and calculations. Some key electronic properties such as highest occupied molecular orbital (HOMO) and lowest unoccupied molecular orbital (LUMO) energies, gap energy, dipole moment and surface area, were calculated and discussed. The various approaches adopted in this study were in reasonable agreement and the following average inhibition efficiency trend was obtained: NNHPE (75.7 %) > NHPE (68.3 %) > PGE (64.2) > MEA (61.0).

Keywords: Synthesis · FTIR spectroscopy · Corrosion inhibition · Theoretical modeling

1 Introduction

Mild steel is a common structural material applicable in a wide range of industries due to its low cost and ease of fabrication. In most industrial processes, acidic solutions are commonly used for cleaning, pickling, descaling, oil well acidizing, etc [1–3]. Corrosion defence had previously been accomplished by conventional methods such as pH control, use of phosphates or chromates, or addition of ammonia. Today, a large number of corrosion inhibitors are in use and there is continuous increase in the number of systems being preserved [4–8]; the final choice being dictated by cost and environmental regulations. Several published works agree that the most effective corrosion inhibitors are those organic compounds containing heteroatoms such as oxygen, nitrogen, sulphur, or multiple bonds and or pi-electron systems in their structures-so called adsorption inhibitors [9–19]. The efficiency of an adsorption inhibitor is mainly dependent on its ability to get adsorbed onto the metal surface, which involves the replacement of water molecules at the corroding metal/solution interface [20].

The search for new and more effective corrosion inhibitors requires the clarification of interactions between inhibitor molecules and metal surfaces [20–23]. Quantum chemical methods have recently become an indispensable tool in the development of new and more functional materials [24,25]. Once a relationship between the structure and reactivity is identified, any number of compounds, including those not yet manufactured, can be readily screened [24–30]. Many scholars beleve that multiactive compounds with large molecular volume tend to give better inhibition performance [31]. This study represents the first fruit of our venture into designing novel, cost effective and ecofriendly inhibitor molecules. Two amine adducts; N-(2-hydroxy-3-phenoxy) ethanolamine (NHPE), N,N-di-(2-hydroxy-3-phenoxypropyl) ethanolamine (NNHPE) were synthesized and tested for their effectiveness and mode of action during mild steel corrosion in 1 M HCl solution using experimental and theoretical approaches. These compounds containing (2-hydroxy-3-phenoxypropyl) amino groups available in literature are known as blocking agents and/or inotropic agents and are useful in the treatment of heart disease such as arrhythmias, angina pectoris, heart failure and hypertension [32]. This is the first of their application for corrosion inhibition purposes. Furthermore, the synthesized amine adducts are non-toxic and environmentally friendly since they are widely used in medicine and have the potential to become green corrosion inhibitors.

[a] Dr. C. O. Akalezi, Dr. F. C. Onwumere, Dr. C. O. Alisa, M. N. Nnanyereugo, Prof. E. E. Oguzie
Department of Chemistry, School of Physical Sciences, Federal University of Technology, PMB 1525 Owerri, Imo State Nigeria
E-mail: chrisakalezi@yahoo.com
christogonus.akalezi@futo.edu.ng
[b] Dr. C. O. Akalezi, Prof. E. E. Oguzie
African Centre of excellence in Future Energies in electrochemical Systems, Federal University of Technology, PMB 1525 Owerri, Imo State Nigeria

2 Materials and Method

2.1 Material

Monoethanolamine (MEA), phenyl glycidyl ether (PGE), NaOH and $MgSO_4$ were used as obtained from Sigma Aldrich, UK. Analytical grade ethanol (from Merck, India) was dried with magnesium sulphate and then vacuum-distilled before use.

2.2 Preparation of N-(2-hydroxy-3-phenoxy) Ethanolamine (NHPE), N, N-Di-(2-hydroxy-3-phenoxypropyl) Ethanolamine (NNHPE)

N-(2-hydroxy-3-phenoxy) ethanolamine (NHPE) was prepared in this wise [33]. To a solution of phenyl glycidyl ether (0.1667 mol) and monoethanolamine (0.1668 mol), ethanol (100 mL) was added. The reaction mixture was allowed to boil under refluxed for 6 hours. For N,N–Di -(2-hydroxy-3-phenoxypropyl), phenyl glycidyl ether 2× (0.1667 mol) and monoethanolamine (0.1668 mol), with 100 mL ethanol respectively were used. The solution was allowed to boil under reflux for 6 hrs. After cooling, the solid products were filtered and recrystallized from methanol. The final product was vacuum filtered, then kept to dry in the desiccator.

2.3 Characterization of the Synthesized Amines

2.3.1 Fourier Transforms Infrared (FTIR) Spectroscopy

The determination of chemical functional groups present in the compounds was achieved using a Thermo Fisher Scientific Nicolet Avatar 380 FTIR Spectrometer. A small quantity of diluted product was directly deposited onto the sample disk, creating a thin film. A spectrum was scanned in the range of 4000 to 700 cm^{-1} interval. Each analysis was repeated twice to detect the characteristic peaks and their functional groups

2.4 Gravimetric Study

Mild steel specimen with dimensions 30 mm × 30 mm, obtained from the Materials and Metallurgy Department, School of engineering FUTO, were utilized for the gravimetric study. The weight percent bulk composition of the steel were: Fe = 99.21; C = 0.21; Si = 0.38; P = 0.09; S = 0.05; Mn = 0.05; and Al = 0.01. The steel samples were used as supplied without further processing. Triple distilled water was used in all tests. Test vessels were 250 mL beaker containing 200 mL of test solution. To avoid turbidity, the test inhibitors were introduced into the electrolyte as solutes in ethanol at 1 % ethanol to the solution volume. The specimen were then inserted without interruption 24 hours under normal aeration. The test procedure was repeated in presence of various concentration test inhibitors.

The weight loss values and inhibition efficiency (%IE) were calculated using Eq. 1 [15].

$$\Delta W = \frac{w_{o-}w_1}{w_o};\ IE\% = \Delta W x\ 100 \quad (1)$$

where, w_o is the weight loss value in the absence of synthesized products (inhibitor), and w_1 is the weight loss values in the presence of inhibitors. The weight loss values reported were the average of three replicate measurements

2.5 Electrochemical Measurement

Electrochemical measurements are performed with a traditional three-electrode cell using VersaSTAT 3 Potentiostat/Galvanostat interfaced with ZsimpWin impedance modeling software. A carbon electrode and saturated calomel electrodes (SCE) were the auxiliary and reference electrodes, respectively. Test metal samples of mild steel for the electrochemical experiment were machined into cubic specimens and fixed in polytetrafluoroethylene (PTFE) tape in such a way that only 1 cm^2 of surface was left uncovered. Prior to polarization, the system was left undisturbed for 24 hours at 303 K, which was sufficient to attain stable open circuit potential (E_{OCP}). Electrochemical Impedance Spectroscopy (EIS) experiments were performed within frequency range 100 kHz to 10 mHz at 303 K using 10 mV AC amplitude signal at $E_{OCP.}$ Then potentiodynamic polarization measurements were performed by sweeping the potential from ±250 mV vs. E_{OCP} at 0.0334 $mV\,s^{-1}$. The data reported is the average of three replicate measurements.

2.6 Quantum Chemical Calculations

Theoretical calculations were performed using density functional theory (DFT) provided by the DMol3 module available in Model 4.0 Material Studio of Accelrys Inc. All calculations were performed using the Perdew-Wang (PW) exchange correlation functional and a double numerical with polarization (DNP) basis set, since this was the best set available in DMol3 [24–26]. This basis set gives good geometry optimizations [27–30].

3 Results and Discussion

3.1 Scheme of Synthesis

To synthesize the new corrosion inhibitors, the reaction sequence outlined in the Schemes 1 and 2 below were followed starting with commercially available monoethanolamine and phenyl glycidyl ether.

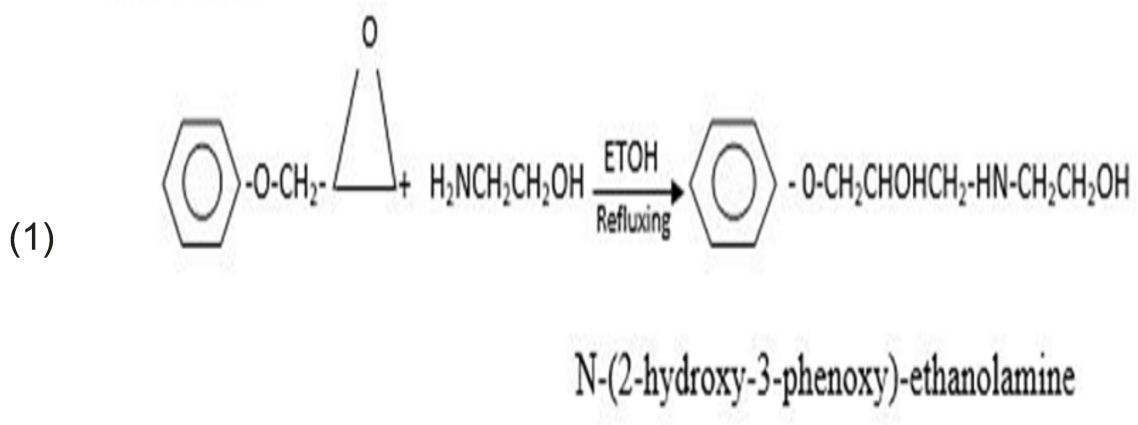

Scheme 1. Synthesis of NHPE.

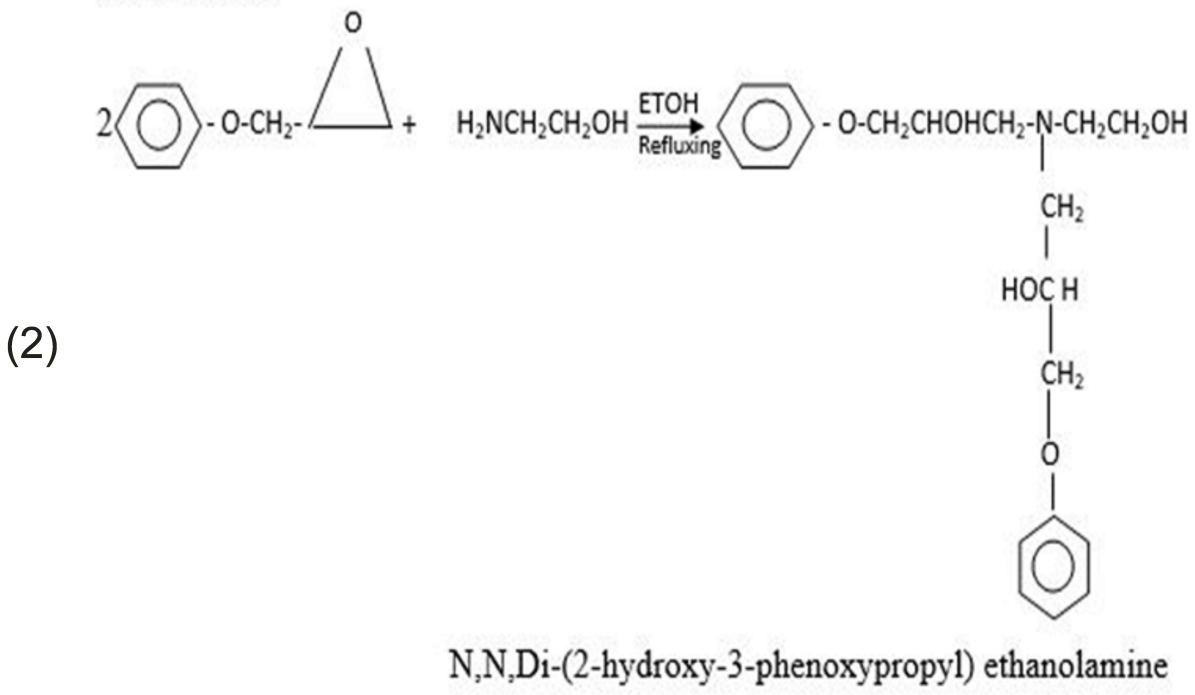

Scheme 2. Synthesis of NNHPE.

3.2 IR Spectra

3.2.1 Analysis of FTIR Spectra Obtained (Product Compounds)

Figures [1 & 2] represents the FTIR spectra of the starting materials (MEA and PGE respectively) which are pure compounds with established spectra. The spectra of NHPE (Figure 3) and NNHPE (Figure 4) reveal the presence of characteristic absorption bands for Ar–C=C–H stretching and bending $–CH_2$ and asymmetrical and symmetrical, –C–Ar–O–C stretching, and epoxy CH_2–(O–CH–) ring stretching vibration. The presence of epoxy groups in the spectra was confirmed with the presence of strong bands at 3,056 cm^{-1} (C–H epoxy) and 913 cm^{-1} (C–O epoxy). The broad doublet peak observed between 3,330–3,200 cm^{-1} is due to the $–NH_2$ vibration absorption of amine compounds. Another doublet peak observed between 1,340–1,370 cm^{-1} is due to the presence of isopropyl group vibration absorption. The –C–N group absorption frequency is seen at 1,117 cm^{-1} for NHPE and 1,034 cm^{-1} for NNHPE. The ether C–O–R is seen at 1,125 cm^{-1}. The aromatic –CH, and –C=C– vibrations are seen around 3,020 and 1,595 cm^{-1} regions for both the amine adducts.

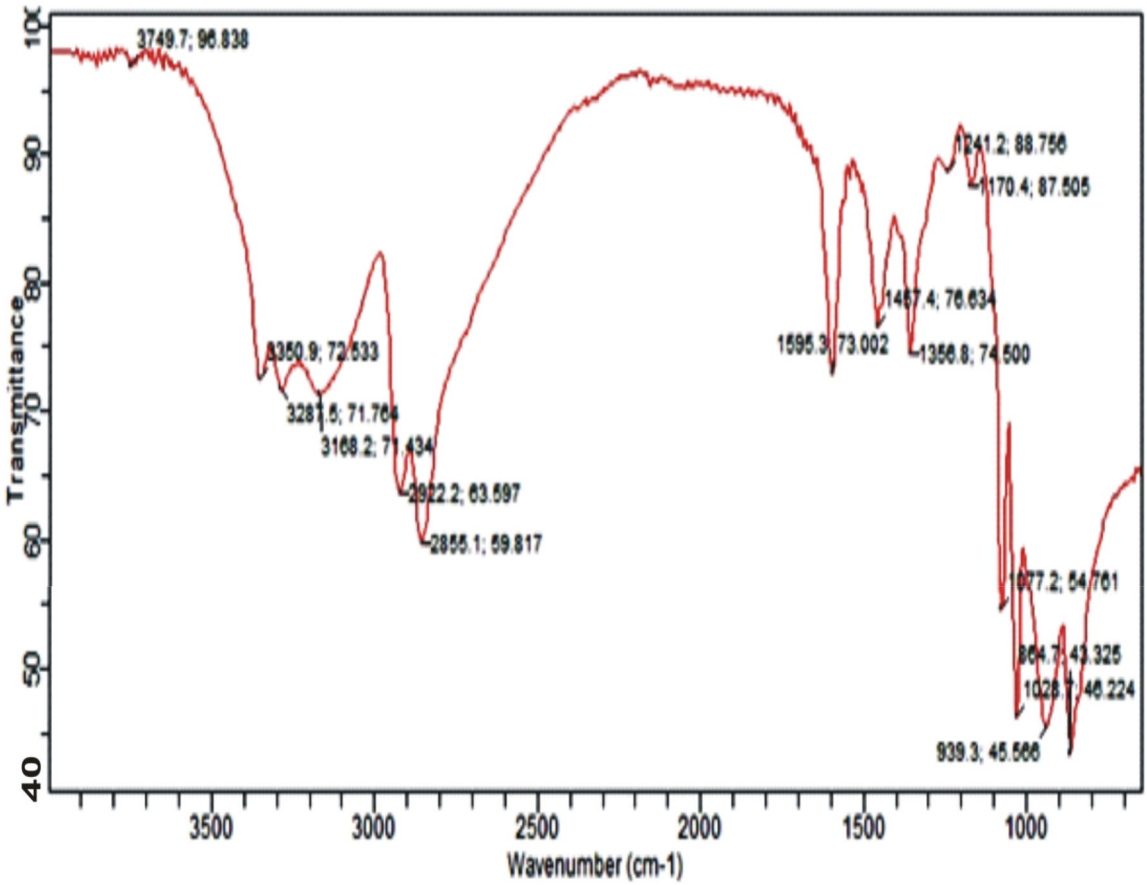

Fig. 1. FTIR spectrum of pure MEA.
This primary amine has two peaks at 3350 and 3293 cm^{-1} typical of O–H and N–H absorptions. Two peaks at 2927 and 2864 cm^{-1} is representative of C–H stretching. The stretch of primary amine results in a band in1601 cm^{-1} and $–H_2C–OH$ between 1461 and 1355.

3.3 Gravimetric Study

Assessment of the results presented in Table 1 shows that inhibition effectiveness of the investigated compounds increased with expanding of concentrations. Figures 5 and 6 respectively represents the plot of decreasing weight loss and increasing inhibition efficiencies with increasing concentration of inhibitor. According to the IE% values obtained in this study, the inhibitor effectiveness of the test inhibitors can be given in the following order: NNHPE > NHPE > PGE > MEA. Highest values obtained being 76.7, 63.1, 55.9, and 49.1 at 0.5 mg/L respectively.

3.4 Electrochemical Measurements

3.4.1 Potentiodynamic Polarization (PDP) Measurements

The Tafel polarization curves obtained for mild steel in 1 M HCl in absence and presence of as-synthesized amines (NHPE and NNHPE) as well the precursor materials (MEA and PGE) are shown in Figure 7. Inspection of Figure 7, shows that addition of the inhibitors in 1 M HCl solution shifted both the cathodic and anodic branches of the polarization curves to lower values of current density indicating the inhibition of both the hydrogen evolution and mild steel dissolution reactions. These observations depicts the character of an inhibitor a mixed-type with a predominant effect on the hydrogen reaction in view of the slight displacement towards the cathodic arm. In an acidic medium, other phenyl amine/heterocyclic corrosion inhibitors having similar results with regard to steel corrosion, have been reported [34–36]. Table 2 represents the derived polarization parameters, i.e. corrosion potential (E_{corr}), cathodic (βc) and anodic (βa) Tafel slopes, corrosion current density (I_{corr}), and the inhibition efficiency (P%) for mild steel corrosion with and without the additives. In particular, the estimated corrosion current (I_{corr}) for blank is 387.49 μA cm^{-2}, which is rapidly reduced to 125.4 and 131.06, 128.93 and 101.99 μA cm^{-2} for MEA, PGE, NHPE and NNPHE at concentration of 0.5 mg/L, respectively. The inhibition efficiency (P%) was calculated from polarization measurements according to the equation given below [15]:

$$P\% = \frac{I^{o}_{corr} - I_{corr}}{I^{o}_{corr}} x100\,\% \quad (2)$$

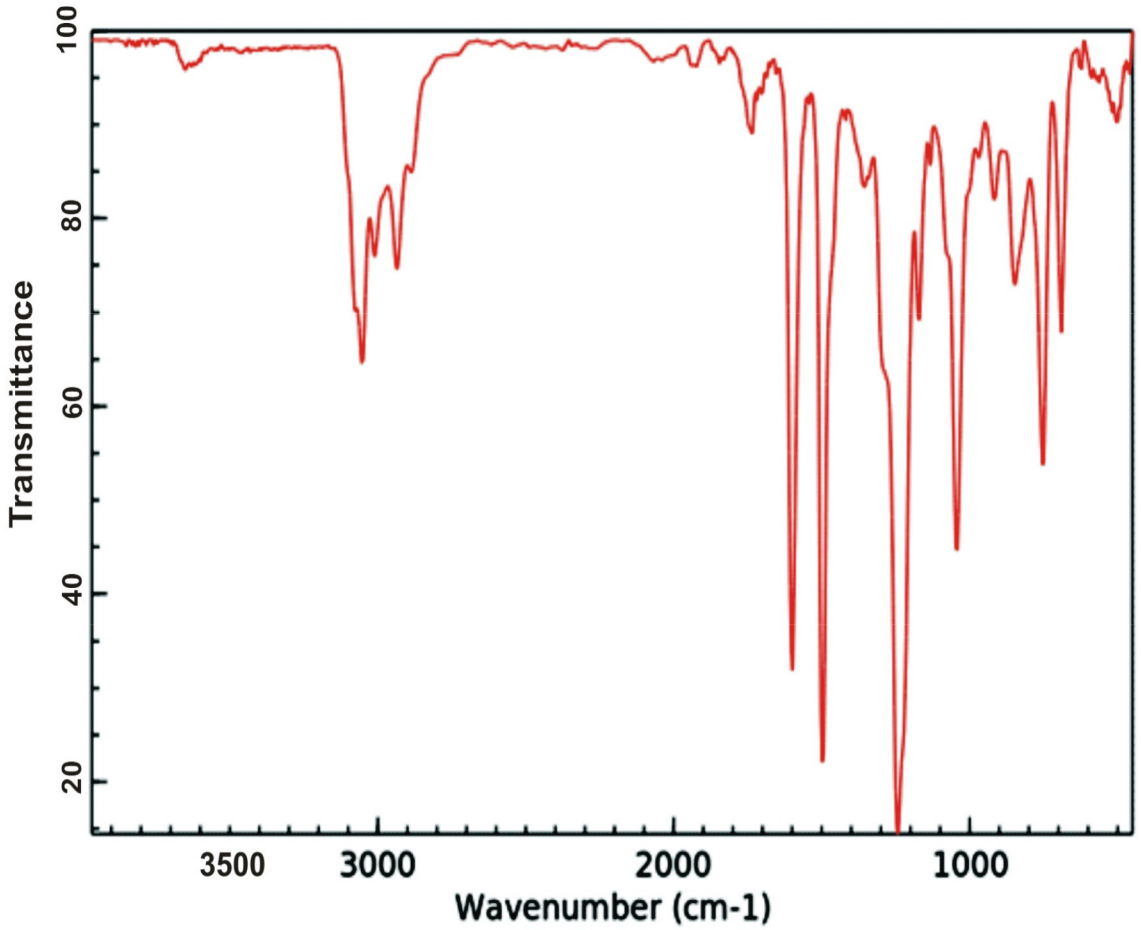

Fig. 2. FTIR spectrum of pure Phenyl Glycidyl Ether (PGE). **(NIST Chemistry Webbook (https://webbook.nist.gov/chemistry)** The peak at 3056 is representative of epoxy –CH–O–CH_2) epoxy, stretch. The peaks at 2,925, 2,967 is representative of –CH_2–, –CH_3– assym stretch. While those at 2,855, 2,872 represents –CH_2–, –CH_3– sym stretch. The peaks at 2,000–1,600 are attributable to Ar–C–H overtone.

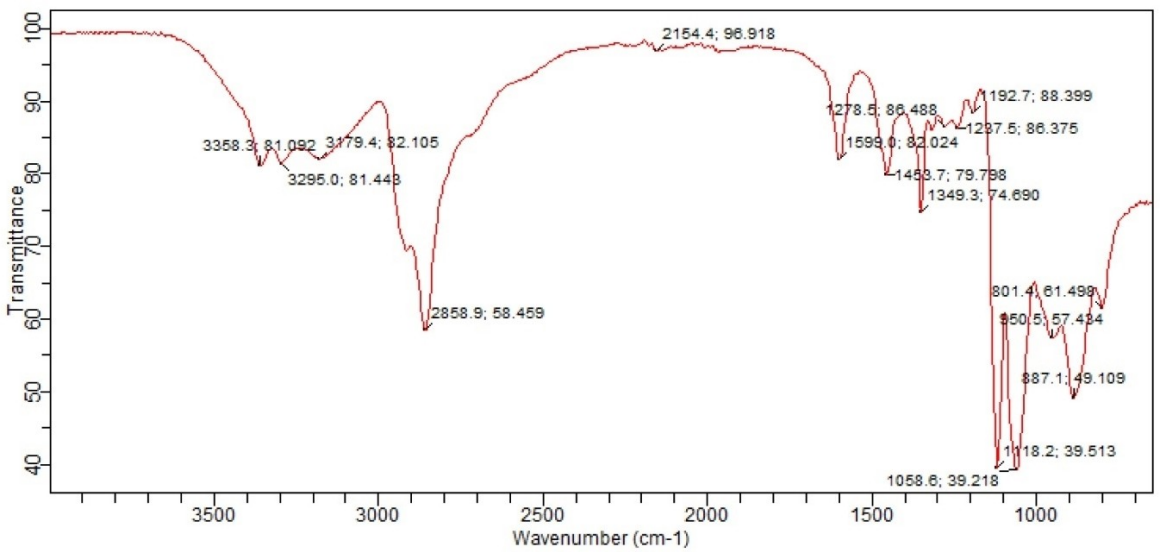

Fig. 3. FTIR spectrum of N-(2-hydroxy-3-phenoxypropyl) ethanolamine.
Here an N–H peak is seen at 3385.8 cm^{-1} and a broad peak in the range 3400 and 3300 cm^{-1} signifies O–H (secondary). Aromatic ring has peak in the range of 1450–1600 cm^{-1}, and the 3 absorption peaks at 1599.0 cm^{-1}, 1494 cm^{-1}, 1457 cm^{-1} signify phenyl absorption.

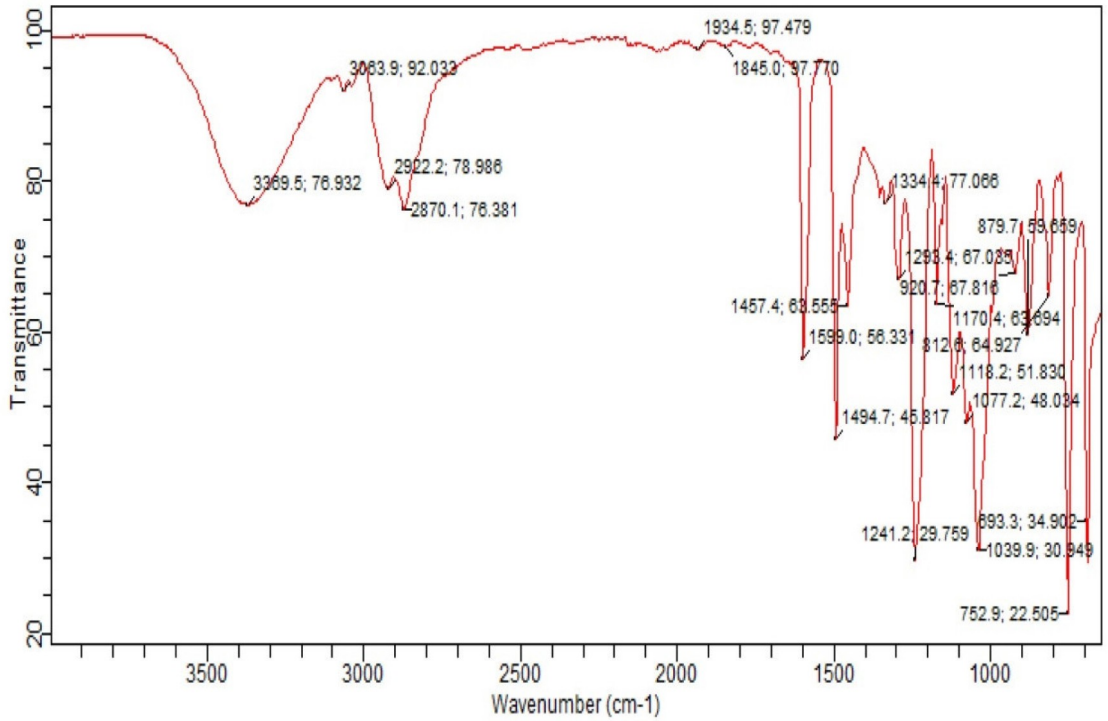

Fig. 4. FTIR spectrum of N,N–Di-(2-hydroxy-3-Phenoxypropyl) ethanolamine.
The peaks at 1334.4 cm^{-1}, 1293.4 cm^{-1}, 1250 cm^{-1} are representative of C–O stretching. Aromatic ring (phenyl) peaks are seen in 1599.0 cm^{-1}, 1494.7 cm^{-1}, 1457.4 cm^{-1} region, while N–C variable stretching seen at 1039.9 cm^{-1},1077.2 cm^{-1}, 1170.4 cm^{-1} as it is expected to absorb in the range of 1020–1360 cm^{-1}

Table 1. Gravimetric data for mild steel corrosion inhibition in presence of MEA, PGE, NHPE and NNHPE in 1 M HCl for 24 hours at 303 K.

Inhibitor	Concentration (mg/l)	Weight loss (mg)	%IE
Blank	0	0.9788 (0.04894)	–
MEA	0.1	0.7641 (0.03821)	28.2 (1.41)
	0.2	0.4191 (0.02095)	40.8 (2.04)
	0.3	0.4352 (0.02176)	42.0 (2.1)
	0.4	0.3501 (0.01751)	46.7 (2.335)
	0.5	0.3172 (0.01586)	49.1 (2.455)
PGE	0.1	0.3443 (0.01722	46.9 (2.345)
	0.2	0.3162 (0.01581)	49.1 (2.455)
	0.3	0.3050 (0.01525)	50.1 (2.505)
	0.4	0.2498 (0.01249)	54.6 (2.73)
	0.5	0.2340 (0.0117)	55.9 (2.795)
NHPE	0.1	0.2894 (0.01447)	56.3 (2.815)
	0.2	0.2804 (0.01402)	57.4 (2.87)
	0.3	0.2341 (0.01171)	60.9 (3.045)
	0.4	0.2150 (0.01075)	62.4 (3.12)
	0.5	0.2062 (0.01031)	63.1 (3.155)
NNHPE	0.1	0.2482 (0.01241)	69.5 (3.475)
	0.2	0.2467 (0.01234)	69.8 (3.49)
	0.3	0.2195 (0.01097)	72.1 (3.605)
	0.4	0.1716 (0.00858)	76.1 (3.805)
	0.5	0.1625 (0.00813)	76.7 (3.835)

Where I^{o}_{corr} and I_{corr} are the corrosion current in the absence and in the presence of inhibitor, respectively.

3.4.2 Electrochemical Impedance Spectroscopy (EIS)

To get further information concerning the inhibition process and to confirm the gravimetric and Potentiodynamic polarization experiments, impedance measure-

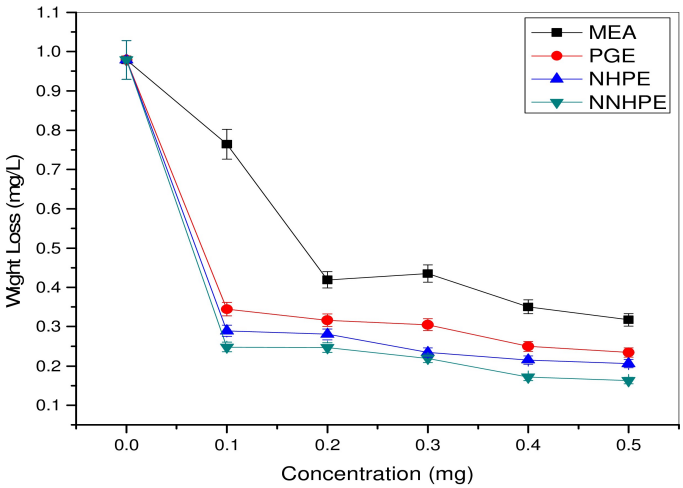

Fig. 5. Relationship between weight loss and different concentrations of the inhibitors in 1 M HCl for 24 hours at 303 K.

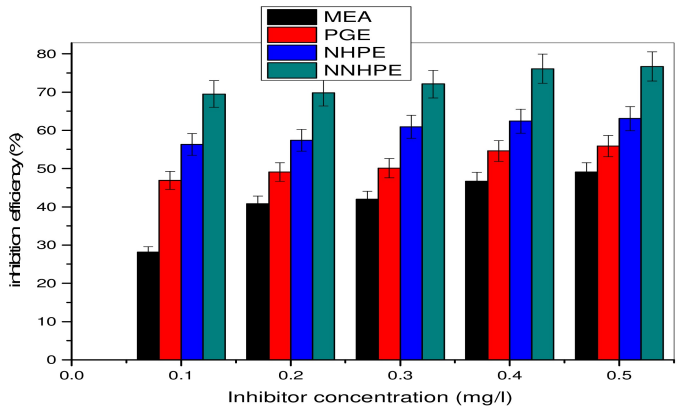

Fig. 6. Relationship between inhibition efficiency (IE %) and different concentrations of the investigated inhibitors for 24 hours at 303 k.

ments were performed on the mild steel electrode at E_{OCP}. Figure 8 shows the obtained Nyquist plots which indicate that the impedance response of mild steel in 1 M HCl solution was significantly changed after the addition of the inhibitor compounds. Evidently from Figure 8(a, b) the Nyquist plots show one depressed semicircular capacitive loop, implying that the charge transfer process involved only a single time constant. The depressed semicircular capacitive loop, plus the noticeable spicks can be attributed to surface roughness and other inhomogeneity of the electrode; phenomenon often referred to as frequency dispersion [37–39]. Table 3 summarizes the obtained EIS parameters. The double layer capacitance (C_{dl}), was determined from the frequency (f), at which the imaginary component of the impedance (Z_i) is maximum (Z_{max}) following Eq.3 [40]:

$$C_{dl} = \frac{1}{2\pi f_{max}} \cdot \frac{1}{R_t} \quad (3)$$

Charge transfer resistance Rt was calculated from high and low frequency impedance data following equation (4) [15].

$$R_t = Z_{re(at\ low\ frequency)} - Z_{re(at\ high\ frequency)} \quad (4)$$

Finally, the percentage inhibition efficiency ($\eta\%$) was calculated from the values of R_t according to the equation (5) [15]:

$$\eta\% = \left(R_t - R_t^o / R_t\right) x100 \quad (5)$$

Where R_t *and* R_t^o are the charge transfer resistance values with and without the inhibitor respectively.

To analyze the impedance spectra, the equivalent circuit (EC) given in Figure 9 was used, where Rs represents the solution resistance, R_t represents the

Table 2. Electrochemical parameters obtained from PDP measurements for mild steel in 1.0 M HCl in absence and presence MEA, PGE, NPHE, and NNPHE (0.5 mg/L respectively) at 303 K.

System	E_{corr}(mV)	i_{corr}(μA)	B_a(mV)	-B_c(mV)	P(%)
Blank	−453.96	387.49	159.39	181.16	–
MEA	−496.54	125.4	208.41	632.42	63.6
PGE	−512.43	131.06	174.1	408.33	65.2
NHPE	−522.7	128.93	181.93	394.23	71.7
NNHPE	−479.9	101.99	139.83	289.49	73.7

Table 3. Impedance parameters of mild steel in 1 M HCl at 303 K in the absence and presence of the synthesized inhibitors.

System	R_s (Ω cm^2)	R_{ct} (Ω cm^2)	N	Q_{dl} (μ Ω^{-1} $s^n cm^{-2}$)	η(%)	Z_{max}
Blank	2.274	103.911	0.812	460.902	–	
MEA	1.733	553.522	0.837	101.311	81.201	69.728
PGE	1.889	741.7012	0.855	77.303	86.001	71.504
NHPE	1.644	671.001	0.869	65.712	84.511	73.087
NNHPE	2.009	696.514	0.885	50.551	85.112	74.910

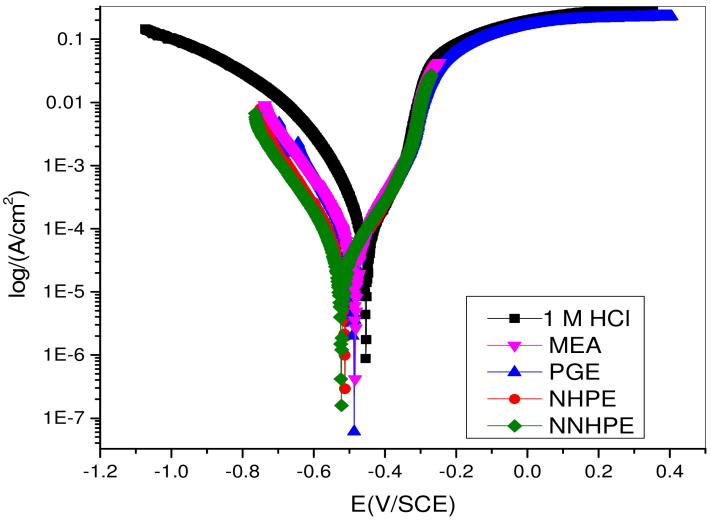

Fig. 7. PDP curves mild steel corrosion in 1.0 M HCl in absence and containing MEA, PGE, NHPE and NNPHE (0.5 mg/L respectively) at 303 K.

charge transfer resistance and C_{dl} represents the electrochemical double layer capacitance. In fact, the presence of inhibitor enhanced the values of the transfer resistance in acidic solution for all the additives. Values of the double layer capacitance are also brought down to the minimum extent in the presence of inhibitor. The trend of inhibition efficiency follows the order similar to that obtained for gravimetric and PDP measurements. The decrease in C_{dl} is due to the adsorption of these compounds on the metal surface leading to the formation of a film against the acidic solution [41,42].

Table 4 compares the percent inhibition efficiencies obtained from the gravimetric and electrochemical techniques used in this study. As is evident from Table 4, the higher values were obtained from the two electrochemical technique, the trend is the same: NNHPE > NHPE > PGE > MEA. NNHPE however, gave a more consistent result with the three techniques.

On a general note, the most realistic corrosion tests are weight loss measurements after exposure. However, they are very slow (weeks, months, or years). On the other hand, electrochemical techniques are rapid. They can measure very low corrosion rates, and give more specific information about the corrosion system or more comprehensive description of the system [43].

Table 4. Comparison of the percent inhibition efficiencies obtained from the various techniques used in this study.

Technique	MEA	PGE	NHPE	NNHPE
Weight loss	49.7	55.9	63.1	76.7
PDP	63.6	65.2	71.7	73.7
EIS	69.7	71.5	73.1	74.9
Average IE%	61	64.2	69.3	75.7

3.5 Quantum Chemical Study Results

With the help of the recent advances in computational chemistry, the effectiveness of an inhibitor can now be related to its spatial molecular and electronic structures using the tool of quantum chemistry. In this study quantum chemical method was introduced to understand the correlation between the molecular structures and inhibition behaviour of the compounds under investigation. Dmol3 module available in Material studio was utilized to assess the frontier molecular orbital density distributions as presented in Figures 10 and 11. Further quantum chemical analysis was carried out to determine such quantum chemical parameters as energy of highest occupied molecular orbital (E_{HOMO}), energy of lowest unoccupied orbital (E_{LUMO}), the gap energy ($\Delta E = E_{LUMO} - E_{HOMO}$) and the dipole moment (μ). A total of eleven parameters were assessed as presented in Table 5.

The value of ionization potential (I) and the electron affinity (A) was obtained from E_{LUMO} and E_{LUMO} using the following relationships according to Lukovits theorem [44–50]:

$$I = -E_{HOMO} \quad (6)$$

$$A = -E_{LUMO} \quad (7)$$

The values of the electronegativity (χ) and the chemical hardness (η) were evaluated using the following relations [50,51]:

$$\chi = \frac{I + A}{2} \quad (8)$$

$$\eta = \frac{I - A}{2} \quad (9)$$

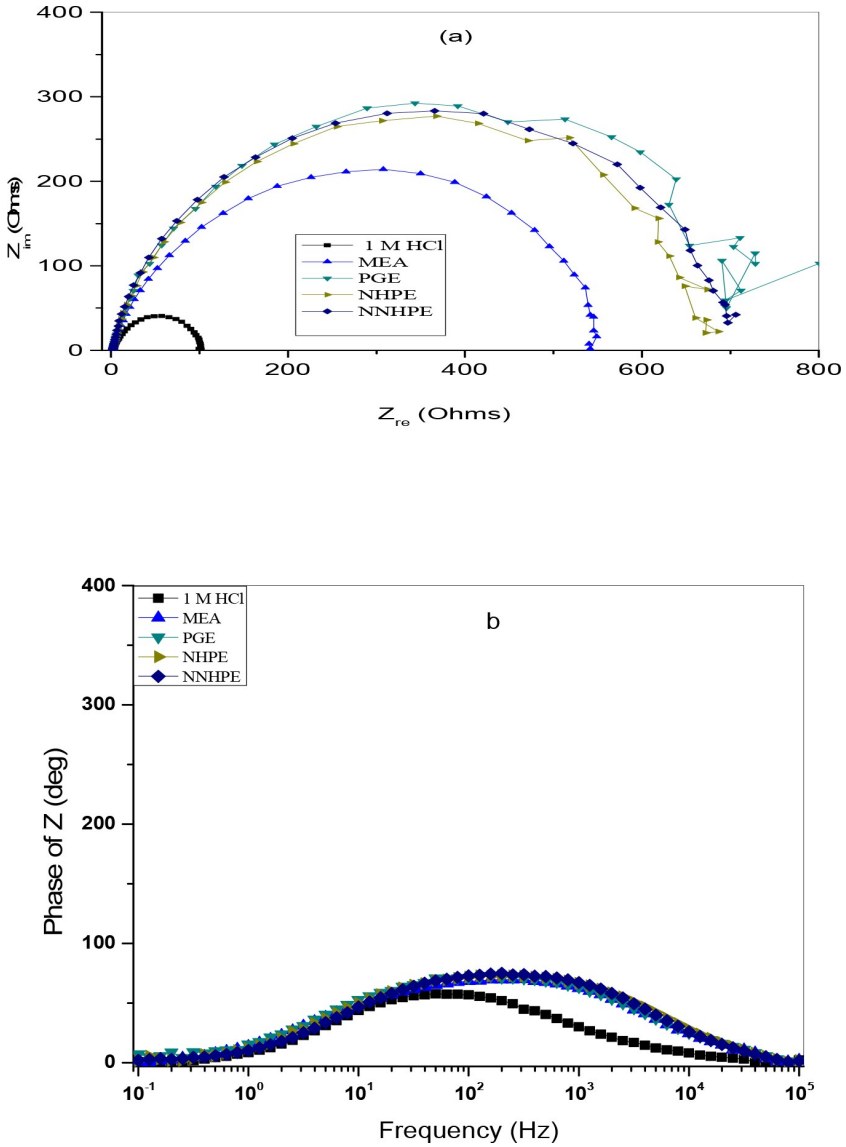

Fig. 8. (a) Nyquist and (b) Bode plots for carbon steel in 1 M HCl in absence and presence of MEA, PGE, NHPE and NNHPE (@ 0.5 mg/L) at 303 K.

Table 5. Electronic and structural parameters for MEA PGE, NHPE and NNHPE employing DFT approach.

Quantum parameters	MEA	PGE	NHPE	NNHPE
E_{HOMO} (eV)	−5.459	−5.477	−5.000	−4.695
E_{LUMO} (eV)	0.955	−1.031	−1.907	−2.268
ΔE (eV)	6.414	4.446	3.093	2.427
Electronegativity (χ) ($\chi = \frac{I+A}{2}$)	3.149	3.254	3.4535	3.4815
Global hardness (η) ($\eta = \frac{I-A}{2}$)	2.272	2.223	1.5465	1.2135
chemical softness (σ) $\sigma = \frac{1}{\eta}$	0.4396	0.4498	0.6466	0.8241
Molecular weight (MW) g/mol	61.083	150.177	211.260	361.437
Total surface area (TSA) $(A^{o})^2$	97.931	184.860	266.358	421.654

Global softness (σ), describes the capacity of an atom or group of atoms to receive electrons which in this study was estimated by using the equation [52]:

$$\sigma = \frac{1}{\eta} = -\frac{2}{E_{HOMO-E_{LUMO}}} \quad (10)$$

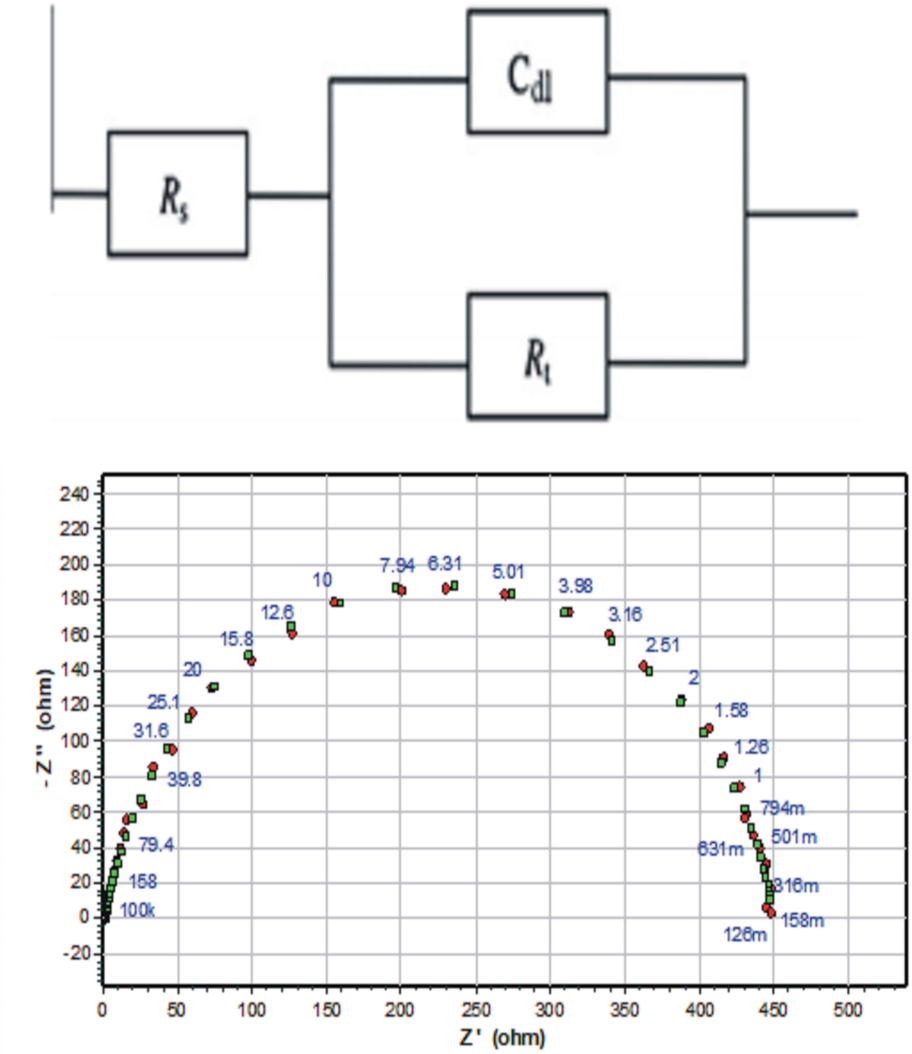

Fig. 9. Representative plot of EIS data fitting of mild steel in 1 M HCl. (**Red points** = **Experimental data**; **Green points** = **Model data**)

Generally, these indices are used to analyze the effect of different substituent on the corrosion inhibition characteristics of a particular parent organic compound.

According to the frontier molecular orbital theory, E_{HOMO} is associated with the electron donating ability of a molecule, and, hence, higher values indicate better inhibition efficiency. Similarly, E_{LUMO} represents the ability of a molecule to accept electrons, and, consequently, lower values of E_{LUMO} can cause higher inhibition efficiency [18,42–45]. In the same way low values of the energy gap ($\Delta E = E_{LUMO} - E_{HOMO}$) will render good inhibition efficiencies, because the energy needed to remove an electron from the last occupied orbital will be low [42–45].

In this study, the order of increasing the values of E_{HOMO} gap (ΔE): NNPHE > NPHE > MEA > PGE.

The order decreasing the E_{LUMO} and the gap energy is more akin to or earlier conclusions: NNPHE > NPHE > PGE > MEA.

This slight deviation of the E_{HOMO} from the earlier trend obtained with the experimental techniques, is not totally surprising; the correlation is not always perfect depending on the computational package (basis set). However, the order obtained here shows that as the size/volume of the molecule increased from MEA and PGE and more importantly from NHPE and NNHPE, the HOMO energy (E_{HOMO}) boosted while the LUMO energy (E_{LUMO}) and the energy gap (ΔE) dropped sharply; pointing to the order of increasing inhibition efficiency.

Absolute hardness and softness, a key properties used to measure the molecular stability and reactivity of a molecules was also determined [45]. Chemical hardness fundamentally signifies the resistance of a molecule towards the deformation or polarization of the electron cloud of a neigbouring atoms, ions or molecules during a chemical reaction. Normally, the inhibitor with the least value of global hardness (hence the highest value of global softness) is expected to have the higher inhibition

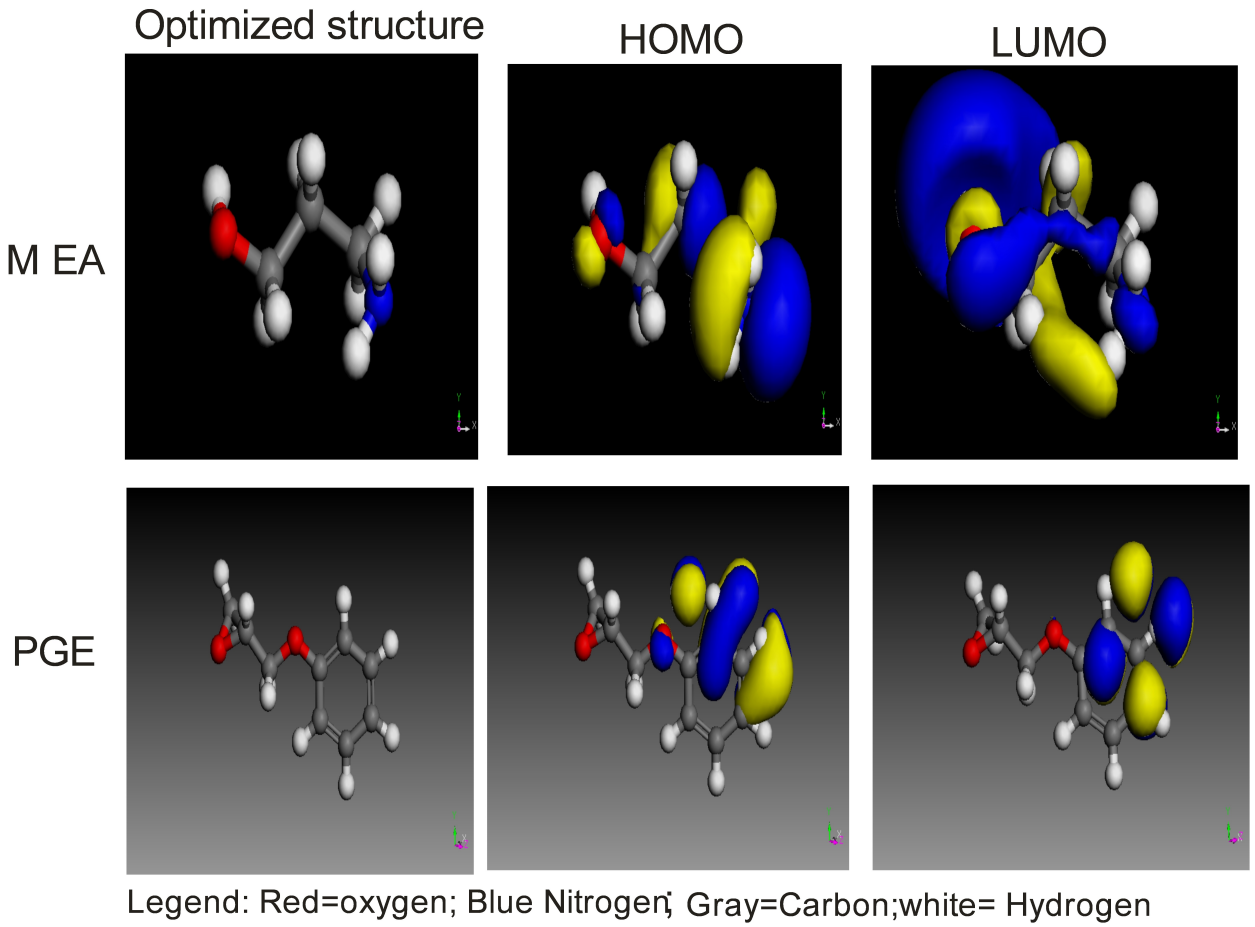

Fig. 10. Optimized structures, HOMO and LUMO orbitals of MEA and PGE MEA is essentially a linear molecule with HOMO and LUMO evenly spread on the entire molecule while those of PGE is centered on the phenyl ring.

efficiency. According to this study, the trend of softness/hardness is thus; (1) Hardness: MEA > PGE > NHPE > NNHPE and (2) Softness: MEA < PGE < NHPE < NNHPE.

Electronegativity is a key parameter used extensively to make predictions about chemical behaviour. In the reaction of two systems with different electronegativities (as a metallic surface and an inhibitor molecule) the electron flow will be from the molecule with the low electronegativity towards that of a higher value, until the chemical potentials are the same [46]. In other words, large electronegativity values characterize the acceptor and small electronegativity values are found for the donors [47–51]. As the electronegativities of the considered inhibitors are smaller than that of metallic iron (7 eV mol^{-1}), shows that if used as inhibitor for Fe, the flow of electrons will be from the molecule to the metal. Thus, the electronegativity values obtained in this study in increasing order is: MEA < PGE < NHPE < NNHPE.

3.6 Correlation Between Electronic Density and Inhibition Efficiency

It has been previously observed that the structure of a molecule can affect the adsorption by influencing the electron density at the functional groups [6]. Therefore, N, O, S, aromatic rings (π-electrons) are expected to be the active centers which has the strongest ability of bonding to the metal surface. Thus when the frontier molecular orbitals are analyzed it is observed from Figure 10 that for MEA, the highest occupied molecular orbital (HOMO) is located on the nitrogen atom while that of PGE, NHPE and NNHPE (Figure 11) were on the phenyl groups. The oxygen atoms in all the structures were not affected. This observation agrees with an earlier report [53–56] that the presence of more than one functional group can lead to changes in the electron density which in turn could influence its adsorption behavior. Thus the areas containing the phenyl group were the primary sites of the bonding. As shown in Table 5, the values of HOMO energy increased with increasing carbon backbone or molecular volume and inhibition efficiency will be enhanced by increase in HOMO. Therefore, the additional phenyl group on

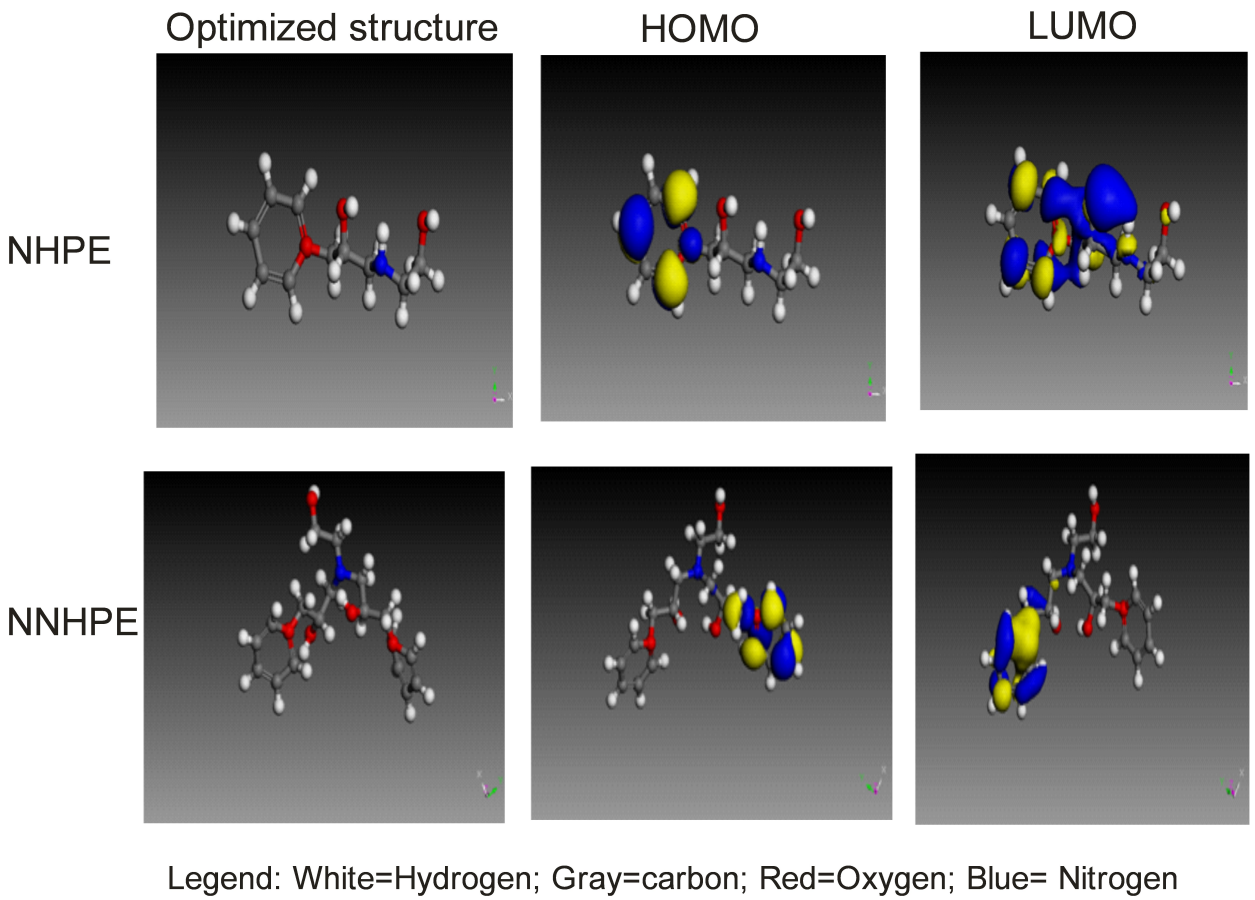

Fig. 11. Optimized structures, HOMO and LUMO orbitals of NHPE and NNHPE.

NNHPE is key to its apparent higher inhibition efficiency in agreement with earlier observations.

The smaller sizes of MEA and PGE (the starting materials) relative to the size of the product amines may result in low surface coverage and consequently leading to less inhibition effect. The increase of surface area leads to better surface coverage and increases the inhibition efficiency. From Table 5, it is clear that the surface area increases as the size of the amine increased from a molecule having only one phenoxy group to that having two. The inhibitor, NNHPE has the higher molecular surface area among the two product amines due to the presence of the additional phenoxy propyl group, which probably makes a better surface coverage of the metal surface and ultimately lead to higher inhibition efficiency.

4 Conclusion

Two new products were successfully synthesized from the reaction between a primary amine, monoethanolamine and phenyl glycidyl ether, following epoxy ring opening reaction mechanism and quantum Chemistry calculations was used for the evaluation of their corrosion inhibition performance. The important findings of the performance evaluation are as follows: Both the starting materials and product amines were characterized using IR spectroscopy and the comparison of the spectra showed that new compounds were produced. As the reaction proceeded, the primary amine adduct are converted to secondary and the tertiary amines. The decrease in the IR band intensity of epoxy groups at about 915 cm^{-1}, as well as at about 3,056 cm^{-1}, was observed due to this process.

The phenyl group dominated the character of the new compounds far more than the hetero atoms and as the complexity of the molecule increased the properties were boosted. Based on the properties assessed the trend of inhibition efficiency is: NNHPE > NHPE > PGE > MEA.

Theoretical and quantum chemical calculation is a powerful tool for estimating inhibitors efficiencies. The theoretical conclusions was authenticated using a gravimetric test method.

Acknowledgements

Support from the World Bank Africa Centers of Excellence for Impact (Ace Impact) project (NUC/ES/507/1/304) is greatly acknowledged

Data Availability Statement

The data that support the findings of this study are available from the corresponding author upon reasonable request.

References

[1] R. T. Loto, C. A. Loto, T. Fedotova, *Res. Chem. Intermed.*, **2013**, *29*, DOI 10.1007/s11164-013-1055-x.
[2] M. Faisa, A. Saeed, D. Shahzad, N. Abbas, F. A. Larik, P. A. Channar, T. A. Fattah, D. M. Khan, S. A. Shehzadi, *Corros. Rev.* **2018**, *36*, 507–545.
[3] M. N. El-Haddad, K. M. Elattar, *Int. J. Ind. Chem.* **2015**, *6*, 105–117.
[4] H. H. Zhang, C. K. Qin, Y. Chen, Z. Zhang, *R. Soc. Open Sci.* **2019**, *6*, 1–19 DOI: 10.1098/rsos.190192.
[5] X. Zheng, S. Zhang, W. Li, M. Gong, L. Yin, *Corros. Sci.* **2015**, *95*, 168–179.
[6] M. Ahmed, M. Al-Sabagh, Notaila, A. A. Nasser, M. A. Farag, M. F. Migahed, Abdelmonem, T. M. Eissa, *Egypt. J. Pet.*, **2013**, *22*, 101–116.
[7] B. Thirumalairaj, M. Jaganathan, *Egypt. J. Pet.* **2016**, *25*, 423–432.
[8] A. M. Abdel-Gaber, B. A. Abd-El-Nabey, I. M. Sidahmed, A. M. El-Zayady, M. Saadawy, *Corros. Sci.* **2006**, *28*, 2765–2779.
[9] A. Singh, M. Talha, X. Xu, Z. Sun, Y. Lin, *ACS Omega*, **2017**, *2*, 8177–8186.
[10] N. A. Negm, A. M. Al Sabagh, M. A. Migahed, H. M. Abdel Bary, H. M. El Din, *Corros. Sci.* **2010**, *52*, 2122–2132.
[11] M. A. Migahed, A. M. Abdul-Raheim, A. M. Atta, M. V. Brostow, *Mater. Chem. Phys.* **2010**, *121*, 208–214.
[12] A. M. Al-Sabagh, H. M. Abd-El-Bary, R. A. El-Ghazawy, M. R. Mishrif, B. M. Hussein, *Egypt. J. Pet.* **2011**, *20*, 33–45.
[13] L. Herrag, B. Hammouti, S. Elkadiri, A. Aouniti, C. Jama, H. Vezin, F. Bentiss, *Corros. Sci.* **2010**, *52*, 3051.
[14] O. Benali, L. Larabi, M. Traisnel, L. Gengembra, Y. Harek, *Appl. Surf. Sci.* **2007**, *253*, 6130.
[15] M. Abd El-raouf, Olfat E. El-Azabawy, R. E. El-Azabawy, *Egypt. J. Pet.* **2015**, *24*, 233.
[16] C. B. Verma, M. A. Quraishi, A. Singh, *J. Inst. Chem.* **2015**, *49*, 229–239.
[17] G. Xia, X. Jiang, L. Zhou, Y. Liao, M. Duan, H. Wang, Q. Pu, J. Zhou, *Corros. Sci.* **2015**, *94*, 224–236. (doi:10.1016/j.corsci. 2015.02.005).
[18] Y. Ji, B. Xu, W. Gong, X. Zhang, X. Jin, W. Ning, Y. Meng, W. Yang, Y. Chen, *J. Inst. Chem.* **2016**, *66*, 301–312.
[19] L. Herrag, B. Hammouti, S. Elkadiri, A. Aouniti, C. Jama, H. Vezin, F. Bentiss, *Corros. Sci.* **2010**, *52*, 3042–3051.
[20] M. A. Migahed, A. A. Attia, R. E. Habib, *RSC Adv.* **2015**, *5*. 57254.
[21] T. Szauer, A. Brandt, *Electrochim. Acta*, **1981**, *26*, 1209–1219.
[22] D. Q. Zhang, L. Gao, G. D. Zhou, *Surf. Coat. Technol.* **2010**, *204*, 1646.
[23] S. Xia, M. Qiu, L. Yu, F. Liu, H. Zhao, *Corros. Sci.* **2008**, *50*, 2021–2029.
[24] G. Gece, *Corros. Sci.* **2008**, *50*, 2981.
[25] A. Chakrabarti, *Br. Corros. J.* **1984**, *19*, 124–126.
[26] K. F. Khaled, N. Hackerman, *Electrochim. Acta.* **2003**, *48*, 2715–2723.
[27] N. Khalil, *Electrochim. Acta.* **2003**, *48*, 2635–2640.
[28] C. Öğretir, B. Mihçi, G. Bereket, *J. Mol. Struct. (Theochem)*, **1999**, *488*, 223.
[29] I. Ahamad, R. Prasad, M. Quraishi, *Mater. Chem. Phys.* **2010**, *124*, 1155–1165.
[30] P. J. Perdew, K. Burke, M. Ernzerhof, *Phys. Rev. Lett.* **1996**, *77*, 3865.
[31] N. Khalil, *Electrochim. Acta.* **2003**, *48*, 2635–2640. (doi:10.1016/S0013-4686(03) 00307-4).
[32] *EUROPEAN PATENT SPECIFICATION*, EP 0 210 849 B1, **29.08.90** Bulletin 90/35.
[33] Manjunath Hegde, S.P Nayak, *JCHPS.* **2018**, *1*, 16–24.
[34] S. A. A. El-Maksound, A. S. Fouda, *Mater. Chem. Phys.*, **2005**, *93*, 84–90.
[35] N. S. Ayati, S. Khandandel, M. Momeni, M. H. Moayed, A. Davoodi, M. Rahimizadeh, *Mater. Chem. Phys.* **2011**, *126*, 873–879.
[36] X. He, Y. Jiang, C. Li, W. Wang, B. Hou, L. Wu, *Corros. Sci.* **2014**, *83*, 124–136.
[37] M. Bouklah, A. Attayibat, B. Hammouti, A. Ramdani, S. Radi, M. Benkaddour, *Appl. Surf. Sci.* **2005**, *240*, 341–348.
[38] A. Ghzaoui, R. Saddik, N. Benchat, M. Guenbour, B. Hammouti, S. S. Aldeyab, *Int. J. Electrochem. Sci.* **2012**, *7*, 7080–7097.
[39] W. W. Zhang, H. J. Li, Y. C. Wu, Q. Luo, H. H. Liu, L. Niu, *Chem. Res. Chin. Univ.* **2018**, *34*, 817–822.
[40] A. P. Yadav, A. Nishikata, T. Tsuru, *Corros. Sci.* **2004**, *46*, 169.
[41] I. B. Obot, N. O. Obi-Egbedi, S. A. Umoren, *Corros. Sci.* **2009**, *51*, 276–282.
[42] P. X. Hui, G. Min, Z. YuXuan, W. Qin, H. B. Rong, *Sci. China Ser. B: Chem.* **2011**, 4332.
[43] N. Thompson, J. Payer, DC Electrochemical Test Methods, *NACE International*, **1998**, ISBN 1-877914-63-0.
[44] K. F. Khaled, N. Kbabić-Samardžiji, N. Hackerman, *Electrochim. Acta.* **2005**, *50*, 2515.
[45] E. E. Oguzie, S. G. Wang, Y. Li, *J. Phys. Chem.* **2009**, *113*, 8420–8429.
[46] J. Tan, L. Guo, H. Yang, F. Zhang, Y. El Bakri, *RSC Adv.* **2020**, *10*, 15163.
[47] E. E. Oguzie, Y. Li, F. H. Wang, *J. Colloid Interface Sci.* **2007**, *310*, 90–98.
[48] J. Fu, S. Li, Y. Wang, L. Cao, L. Lu, *J. Mater. Sci.* **2010**, *45*, 6255–6265.
[49] E. E. Oguzie, C. K. Enenebeaku, C. O. Akalezi, S. C. Okoro, A. A. Ayuk, E. N. Ejike, *J. Colloid Interface Sci.* **2010**, *349*, 283–292.
[50] I. Lukovits, E. Kálmán, F. Zucchi, *Corrosion*, **2001**, *57*, 3–8.
[51] Q. Salam, K. T. Abed, T. S. Gaaz, A. A. Al-Amiery, A. A. H. Kadhum, K. S. Reda, W. K. Ahmed, *Res. Phys.* **2018**, *8*, 1178–1184.
[52] A. Ghame, T. Douadi, S. Issaadi, L. Sibous, K. I. Alaoui, M. Taleb, S. Chafaa, *Int. J. Electrochem. Sci.* **2017**, *12*, 4867–4897.
[53] K. Raja, A. N. Senthilkumar, K. Tharini, *Adv. Appl. Sci. Res.* **2016**, *7*, 150–154.
[54] M. A. Qurashi, R. Sardar, *J. Appl. Electrochem.* **2003**, *33*, 1163–1168 (doi:10.1023/B: JACH.0000003865.08986.fb).
[55] K. F. Khaled, *Corros. Sci.* **2010**, *52*, 3225–3234.
[56] N. Hackerman, E. L. Cook, *J. Electrochem. Soc.*, **1950**, *9*, 1–9.

Received: July 21, 2020
Accepted: October 15, 2020
Published online on ■■, ■■

FULL PAPER

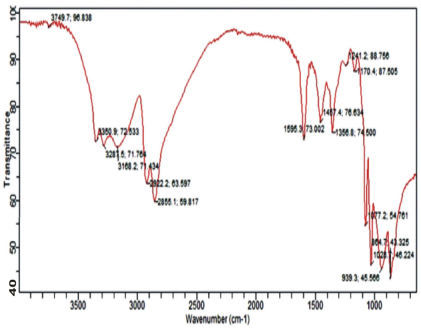

Dr. C. O. Akalezi, Dr. F. C. Onwumere, Dr. C. O. Alisa, M. N. Nnanyereugo, Prof. E. E. Oguzie*